Improvement of Aerodynamic Performance of Cambered Airfoils Using Leading-Edge Slots

Saman Beyhaghi
Department of Mechanical Engineering,
University of Wisconsin-Milwaukee,
3200 N. Cramer Street,
Milwaukee, WI 53211
e-mail: beyhagh2@uwm.edu

Ryoichi S. Amano[1]
Fellow ASME
Department of Mechanical Engineering,
University of Wisconsin-Milwaukee,
3200 N. Cramer Street,
Milwaukee, WI 53211
e-mail: amano@uwm.edu

Feasibility of increasing lift and decreasing drag by drilling narrow span-wide channels near the leading edge of NACA 4412 airfoils is investigated. It is proposed to drill two-segment slots that allow some of the incoming air to flow through them and then exit from the bottom surface of the airfoil. Such slots can result in an increased local pressure and thereby higher lift. Length, width, inlet angle, and exit angle of slots are varied to determine optimum configurations. Aerodynamic performance at different angles of attack (AoAs) and the chord-based Reynolds number of 1.6×10^6 is investigated. It is concluded that longer and narrower slots with exit streams more aligned with the air flowing below the airfoil can result in a higher lift. Also, in order to keep the slotted airfoils beneficial for AoAs greater than zero, it is proposed to (a) slightly lower the slot position with respect to the original design and (b) tilt up the first-leg by a few degrees. For the best design case considered, an average improvement of 8% is observed for lift coefficient over the entire range of AoA (with the maximum increase of 15% for AoA = 0), without any significant drag penalty. [DOI: 10.1115/1.4036047]

Introduction

Although horizontal-axis wind turbines (HAWTs) have proven to be very useful for generating electrical energy, they suffer from some limitations, such as the Betz limit, which confines the efficiency of turbines to around 59% [1]. A great deal of research has been aimed at finding ways to increase the power generation from turbines, by either modifying the airfoil shape or installing add-on features at certain spanwise and chordwise locations of the blades. The objective of those alterations is to change the flow pattern around the airfoil so as to decrease drag and increase lift and ultimately increase the overall power generation. Some of those devices commonly used are suction-side minitabs [2], riblets [3,4], and vortex generators (VGs) [5,6]. Some of the important concerning issues for such additions are manufacturability, durability, drag penalty, and additional fatigue loads.

While active flow control using suction and injections streams is in use, the possibility of using slots for passive flow control is rarely investigated. One application of slots on airfoils is using leading-edge root extension (LERX) devices that are deployed in some modern fighter aircraft. LERX is a small filet that runs forward from the leading edge of the wing. It can generate streamwise vortices that adhere to the top wing surface and, therefore, prevent the boundary layer separation and maintain the lift force at high values at high angles of attack. This method can also be applied to wind turbines. In fact, some variations of it have been deployed by installing suction holes near leading or trailing edge of the airfoil, in order to remove the low-momentum layers of the flow from the bottom of the boundary layer and, therefore, delay the separation [7,8].

The new flow control method discussed in the present work is different than the conventional leading-edge blowing technique, in that the slot exit is located at the bottom surface of the airfoil in the presently investigated cases. Therefore, air flowing through the slot is forced to leave from the pressure-side, meaning the flow direction is opposite of what is traditionally seen. The possibility of using leading-edge slots for horizontal-axis wind turbines has been investigated very rarely. Subash et al. [9] studied the flow over a slotted NREL (airfoil S883) blade. They showed qualitatively that employing slots can alter the pressure distribution above and below the airfoil. There are no quantitative results presented.

In two recent studies at the University of Wisconsin-Milwaukee (UWM), wind turbine blades with leading-edge slots have been tested experimentally. The purpose of using slotted blades was to redirect some of the air flows through the blade, and later mix it with the air stream flowing along the bottom surface of the airfoil [10,11]. Figure 1 shows a small slotted wind turbine blade. NACA 4412 airfoil profile is used throughout the blade span due to its high lift-to-drag ratio. This blade was designed using the CAD software package, Pro/Engineer, then three-dimensional printed, and tested at the UWM Wind Tunnel Laboratory. More detail on the experimental facilities and procedure can be found in Ref. [11].

The performance of the slotted blade is examined experimentally in very limited operating conditions. This blade has shown to

Fig. 1 The slotted wind turbine blade fabricated and tested at UWM Wind Tunnel

[1]Corresponding author.

Contributed by the Advanced Energy Systems Division of ASME for publication in the Journal of Energy Resources Technology. Manuscript received September 27, 2016; final manuscript received February 9, 2017; published online March 16, 2017. Assoc. Editor: Ashwani K. Gupta.

generate on average 26% more power than the standard blade for incoming air speed between 4.5 and 7.7 m/s, and the corresponding tip-speed ratio TSR (defined as $\Omega r/U_\infty$, where r is the blade length in m, and Ω shows the angular velocity in rad/s) increasing linearly from 4.8 to 6.2 [11]. No data are, however, reported beyond these ranges. Therefore, there is a need for further characterization of such slots under various operating conditions.

The objective of the present study is to build upon the previous results and carry out a rigorous parametric study on some of the design parameters. The focus is on airfoils, as opposed to blades because it allows us to characterize the performance under different local angles of attack (AoA). Moreover, the findings can be used on not only wind turbine blades but also airfoils utilized for any other applications such as airplane wings or unmanned aerial vehicles (UAVs). Note the chord-based Reynolds number (Re) is kept constant at $\sim 1.6 \times 10^6$ throughout this study, and AoAs between 0 deg and 16 deg (near-stall condition) with 2 deg increments are selected for this investigation. The computational results of a standard solid airfoil are compared against the experimental data from the literature. A thorough investigation of all geometrical parameters, aerodynamic performance under different Re's, and application of slots to rotating wind turbine blades will be subjects of future studies.

Theory

Transport Equations. To model the turbulent air flow around the slotted airfoil, the Reynolds-averaged Navier–Stokes (RANS) model of k–ω shear stress transport (SST) is used. This model is computationally more affordable than higher-end techniques such as large Eddy simulation (LES) and has gained a lot of attraction among the RANS models. This model is suitable for inner and outer parts of the boundary layers and outside the boundary layer. The SST formulation switches to a k–ε behavior in the free-stream, and therefore, it avoids the common problem often seen with the standard k–ω, which is being too sensitive to the inlet turbulence properties. The governing equations unique to this turbulence model are outlined in Eqs. (1)–(4). More details including the closure coefficients relevant to this model can be found in Ref. [12].

Reynolds stresses

$$-\rho\langle u_i u_j\rangle = \mu_t\left(\frac{\partial U_i}{\partial x_j}+\frac{\partial U_j}{\partial x_i}-\frac{2}{3}\frac{\partial U_k}{\partial x_k}\delta_{ij}\right)-\frac{2}{3}\rho k\delta_{ij} \tag{1}$$

Turbulent eddy viscosity

$$\mu_t = \rho\nu_t = \frac{\rho a_1 k}{\max(a_1\omega, WF_2)}, \quad \text{where} \quad W = \sqrt{2W_{ij}W_{ji}},$$
$$W_{ij} = \frac{1}{2}\left(\frac{\partial U_i}{\partial x_j}-\frac{\partial U_j}{\partial x_i}\right) \tag{2}$$

Turbulent kinetic energy

$$\frac{\partial k}{\partial t}+U_j\frac{\partial k}{\partial x_j} = P_k-\beta^* k\omega+\frac{\partial}{\partial x_j}\left[(\nu+\sigma_k\nu_t)\frac{\partial k}{\partial x_j}\right] \tag{3}$$

Specific dissipation rate

$$\frac{\partial \omega}{\partial t}+U_j\frac{\partial \omega}{\partial x_j} = \frac{\gamma}{\mu_t}P_k-\beta\omega^2+\frac{\partial}{\partial x_j}\left[(\nu+\sigma_\omega\nu_t)\frac{\partial \omega}{\partial x_j}\right] + 2(1-F_1)\frac{\sigma_{\omega 2}}{\omega}\frac{\partial k}{\partial x_i}\frac{\partial \omega}{\partial x_i} \tag{4}$$

Lift and Drag Coefficients. The aerodynamic performance of airfoils is typically quantified using the lift and drag forces exerted on the airfoil surface. A lift coefficient is a dimensionless number that models all of the complex dependencies of shape, inclination, and some flow conditions on the lift. This coefficient indicates the ratio between the actual lift forces (normal to the main flow direction) and the force generated by the dynamic pressure as follows:

$$C_L = \frac{2L}{\rho U_\infty{}^2 A} \tag{5}$$

Similarly, the drag coefficient is a dimensionless number that quantifies drag or the resistance force of the airfoil exposed to the fluid flow. This coefficient comprises the effect of the two primary contributors to drag, i.e., the shear drag caused by the friction forces between the solid surface and the adjacent fluid layers, and the form drag caused by the pressure differences between the upstream and downstream of the airfoil. Drag coefficient is defined as

$$C_D = \frac{2D}{\rho U_\infty{}^2 A} \tag{6}$$

Computational Setup

The computational modeling and analysis are carried out using the commercial computational fluid dynamics (CFD) package, STAR-CCM+. The geometry is developed by importing a standard NACA 4412 airfoil profile in the software, cutting the slot through the airfoil, extruding it to a proper spanwise length, and finally creating the surrounding domain and subtracting the slotted airfoil from it. As for the computational grid, several meshing schemes were examined, including a fully structured (trimmed) grid, polyhedral mesh, and a fully structured body-fitted mesh. After an extensive investigation, it was determined that the polyhedral mesh is a good trade-off between the accuracy and the computational cost. The polyhedral mesh was augmented with 16–18 prism (inflation) layers near the airfoil surface to deliver the proper grid resolution for wall y^+ requirements of the k–ω turbulence model. For one of the slotted airfoils studied, a grid independence study was carried out to find the proper values of the mesh setting parameters. For that particular case, three different grids with 210 K, 560 K, and 950 K polyhedral elements were generated, and the flow was solved for each case to find the lift and drag coefficients. As shown in Table 1, the case with 560 K elements resulted in very similar force coefficients as the finest case, whereas both lift and drag of the coarsest case were roughly 3% different than the other two. Since the objective of the present work is to find an optimal design based on C_L and C_D values, even a few percent difference is considered significant and can make a difference. Based on the observed values for lift and drag coefficients of the three cases considered, the mesh setting parameters of the case with 560 K elements are used for the remainder of this research. Note that the actual element count of the individual cases is highly dependent on the slot's parameters, mainly its width and length.

A coupled pressure-based flow solver with the second-order discretization and the Courant–Friedrichs–Lewy number of 5 was used for simulations, and the under-relaxation factor of 0.8 was assigned for k–ω turbulence. Air with constant properties at $T = 300$ K and $P = 101$ KPa was modeled in all simulations.

Figure 2 depicts the geometry and the mesh configuration chosen for this study. A C-H-shape geometry of grids is selected as the computational domain. All the far-field boundaries are assigned free-stream boundary conditions, and all solid surfaces

Table 1 Mesh independence study in terms of lift and drag coefficients for a slotted airfoil with $L_1/c = 45\%$, $w/c = 2\%$, $\beta_1 = 0$ deg, and $\beta_2 = 80$ deg at AoA = 0 deg

Number of mesh elements	Lift coefficient	Drag coefficient
210,000	0.4503	0.0233
560,000	0.4678	0.0242
950,000	0.4673	0.0242

of the airfoil are given a no-slip wall condition. The free-stream velocity magnitude U is set to 24 m/s, resulting in a chord-based Re of 1.6×10^6. The two side surfaces of the domain are assigned a periodic boundary condition. All simulations are run until a convergence criterion of 1×10^{-6} is achieved for all flow quantities. In Fig. 3, a typical slotted airfoil along with the main geometric parameters of interest is shown. The widths of the first and second legs of the slot are set equal throughout this study. The chord and span lengths are set to 1 m and 0.2 m, respectively. The variable h indicates the vertical (normal to chord) distance between the "mouth" of the slot (bottom-edge of slot's inlet plane) and a fixed point within the airfoil (shown as a small circle, which is $0.4c$ downstream and $0.04c$ above the leading edge).

Primary Results

Results of the initial validation cases along with some of the preliminary results are presented in this section.

Initial Validation. Results of a well-known published experimental study by Wadcock [13] are used for validation of the lift and drag coefficients obtained from CFD simulations of the solid airfoil. The reference above is used by many researchers for validation studies including NASA Langley Research Center for validation of different turbulence models [14]. Lift and drag forces are measured for AoAs between 0 deg and 16 deg with 2 deg increments, and the results are compared against CFD results in Fig. 4(*a*). The agreement between the two data sets is excellent, with only small discrepancies in higher AoAs for the drag coefficient. This trend could be attributed to the increasing importance of unsteady effects in higher AoAs, which will possibly be improved by using higher-order unsteady turbulence models. Moreover, for turbulent flow around a solid airfoil with AoA = 0 deg, the distribution of the pressure coefficient over the airfoil surface at midspan is obtained from CFD and is compared against the available experimental data in Fig. 4(*b*). The good agreement between the two data sets confirms the validity of the CFD formulation and results.

Performance at AoA = 0. In an attempt to determine the optimum geometric configuration of the slot, a series of computational parametric studies were performed, in which three of the geometric properties were independently varied, and lift and drag coefficients were calculated. The variables of interest for these simulations were the first-leg relative length percentage (L_1/c), slot width w (which was always kept identical between the first and second legs of the slot), and the deflection angle of the second leg with respect to the first-leg, β_2. The results of the 14 configurations examined are outlined in Fig. 5. The values of the variables treated as constant in each series of simulations are indicated above the corresponding columns. Note in all of the cases in this section, the slot first-leg angle β_1 is set to zero and $h/c = 4\%$. From Fig. 5(*a*), it is evident that all the simulation cases outperform the solid airfoil case regarding the lift coefficient. This improvement can be as high as 65% for the best case. At a fixed exit angle and slot width, it is shown that lift coefficient increases with L_1. Meanwhile, one can note from Fig. 5(*b*) that C_D decreases as L_1 increases. From the second set of simulations in Figs. 5(*a*) and 5(*b*), it is found that unlike the slot length, the exit angle β_2 does not play a significant role in determination of the lift. However, slots with smaller β_2 result in lower drag forces. Therefore, this angle is recommended to remain small in future investigations. Finally, from the third set of simulations ($L_1/c = 70\%$ and $\beta_2 = 45$ deg), it is found that wider slots will result in slightly higher lift, but also much higher drag as compared to the narrower slots. Therefore, it is recommended to keep the slot width as small as practically possible. In summary, even though all of the chosen cases result in an improved lift, there seems to be an inevitable drag penalty. If one's objective is only to maximize the lift, the fifth case ($\beta_2 = 85$ deg, $w = 2$ cm, and $L_1/c = 90\%$) seems to be the optimum solution. However, if the drag has to be taken into account, the 11th case ($\beta_2 = 45$ deg, $w = 0.5$ cm, and $L_1/c = 70\%$) seems more appropriate *for the cases studied*. Overall, one can conclude that it is better to keep L_1 as large as possible, while keep w and β_2 as small as possible.

Effect of Slot Width and First-Leg Length. All three quantities explored in the previous section, Performance at AoA=0, seem to be somewhat influential in the determination of lift and drag. While other geometric variables can potentially impact the performance, in this section, the variation of lift and drag as a

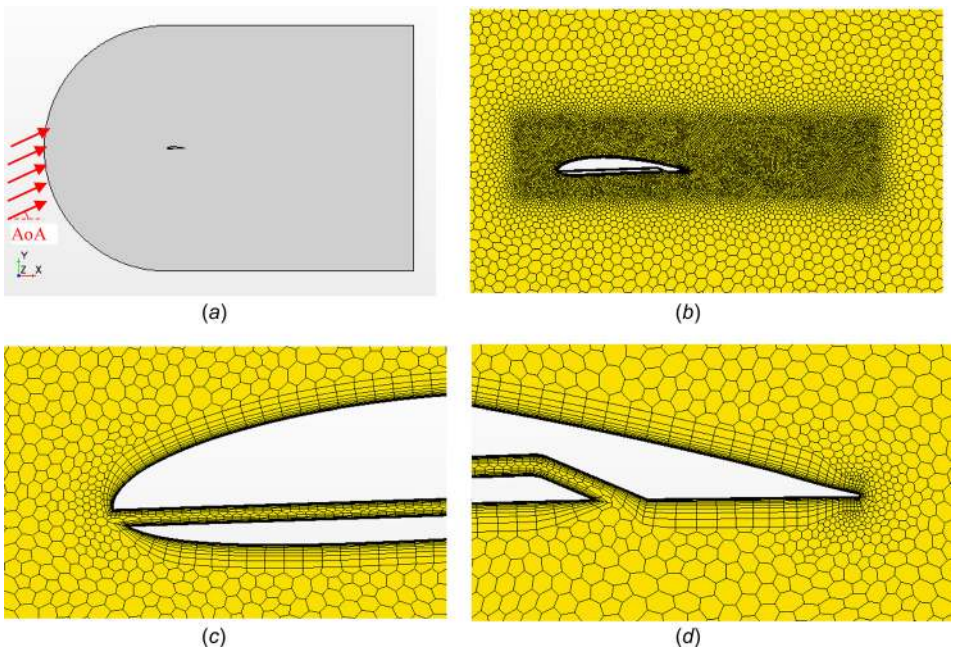

Fig. 2 The computational domain and the mesh generated around a typical slotted airfoil: (*a*) geometry, (*b*) mesh around the airfoil, (*c*) mesh magnified near the leading edge and slot, and (*d*) mesh near the trailing edge

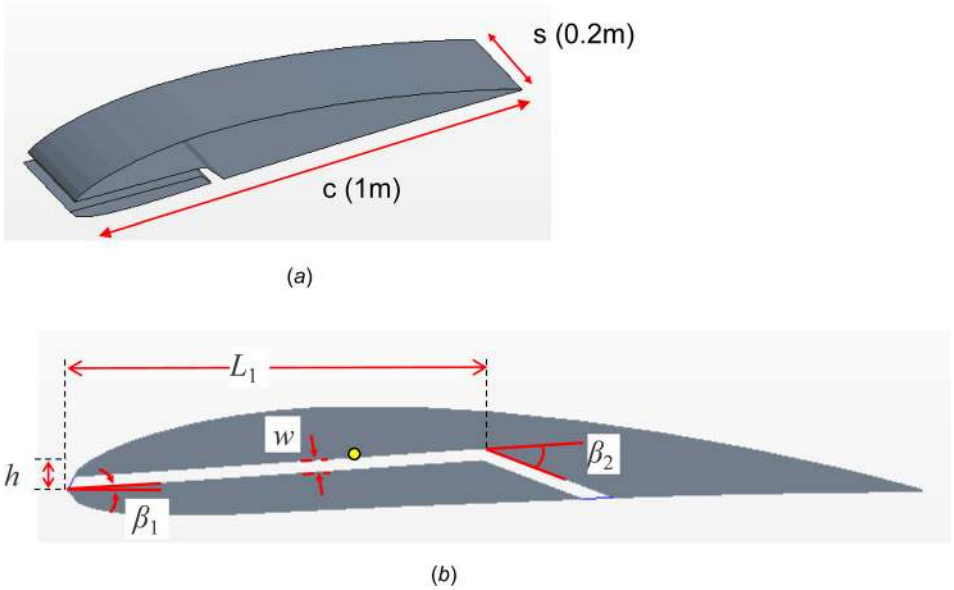

Fig. 3 (*a*) A typical picture of a slotted airfoil considered for this study and (*b*) cross section of a slotted airfoil with five main geometric parameters shown

function of only two variables, i.e., w and L_1, is investigated. Especially, the former is important because it can directly determine the amount of air flowing through the slot and ejecting from the suction side, and therefore, it can alter the pressure distribution and flow dynamics around the airfoil. In Fig. 6, the simulation results for turbulent air flow over a slotted airfoil with four different slot widths are presented. Lift and drag coefficients are obtained for slot widths of 0.5, 1, 2, and 3 cm at AoAs of 0 deg, 2 deg, 4 deg, 6 deg, and 8 deg. Same is reported for a *solid baseline* airfoil without any slot drilled inside. As discussed earlier, all

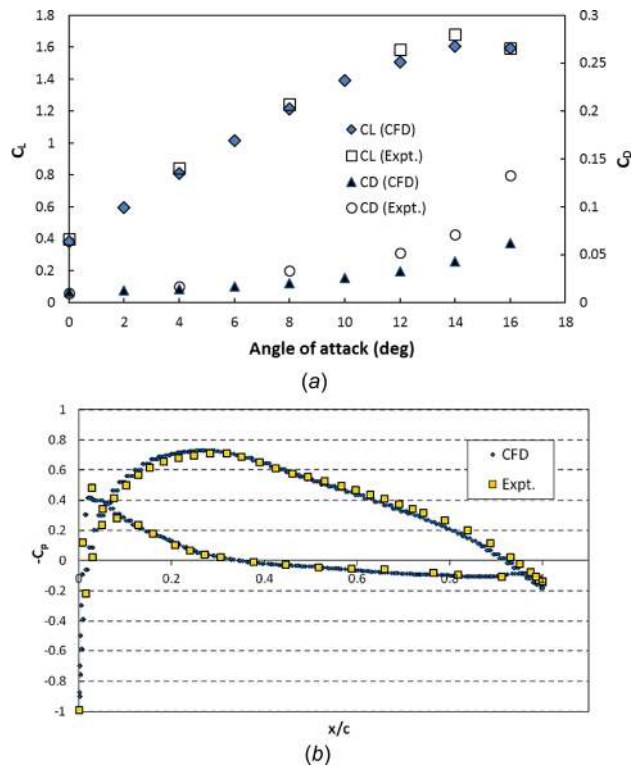

Fig. 4 (*a*) Lift coefficient, (*b*) drag coefficient, and (*c*) pressure coefficient with negative sign at AoA = 0 deg

slot widths prove to be beneficial for improvement of lift at zero AoA, whereas, at AoA = 2 deg, only the three smallest airfoil widths show higher lifts compared to the solid airfoil. As AoA increases, the solid airfoil seems to generate more lift and less drag as compared to any slotted airfoil. This means that using the slots with configurations above cannot improve the aerodynamic performance of NACA 4412 airfoils at $\mathrm{Re} = 1.6 \times 10^6$.

Similarly, the effect of the slot first-leg length L_1 on lift and drag coefficients at $\mathrm{Re} = 1.6 \times 10^6$ is demonstrated in Fig. 7. For AoAs 0 deg and 2 deg, all of the slotted airfoils generate higher lift than the solid one, with the $L_1/c = 90\%$ case showing the best performance. However, at higher AoAs, the solid airfoil shows a better performance, while all five slot lengths considered seem to have the same impact. A similar trend is observed for the drag coefficient, where the solid airfoil comes with the smallest drag, followed by $L_1/c = 90\%$ slotted airfoil, and then the rest of the test cases. One can justify the inferior performance of the aforementioned slotted airfoils at higher AoAs by noting that based on the current vertical position of the slots, incoming air streams cannot enter the slots from the leading edge, and instead they tend to enter the slot from the end. The reverse flow through the slot could alter the pressure distribution over the slot surface and could generate an undesirable downward force that results in smaller lift coefficient. Figure 8 shows the local velocity vectors in the spanwise midplane near the airfoil for the two cases with AoAs of 0 deg and 8 deg. The other slot parameters are as follows: $L_1/c = 70\%$, $w/c = 2\%$, $\beta_1 = 0$ deg, $\beta_2 = 85$ deg, and $h/c = 4\%$. While the flow pattern in the AoA = 0 deg case (Fig. 8(*a*)) is as expected, there exists reverse flow in the AoA = 8 deg case (Fig. 8(*b*)). This happens because in the latter case, the stagnation point is located below the slot's inlet, and therefore the incoming streamlines cannot find their way through the slot. However, the condition for entering through the back end of the slot is quite plausible. This phenomenon explains degradation of the lift at higher AoAs for the cases with $h/c = 4\%$.

Effect of Slot Inlet Angle. To make slots more advantageous for AoAs greater than zero, it is now proposed to adjust the slot inlet angle β_1 according to the incoming flow AoA. In this section, flow around slotted airfoils with different β_1 is simulated at AoA = 4 deg. The results for cases with $\beta_1 = 0$ deg, 4 deg, 8 deg, and 16 deg are listed in Table 2. The $\beta_1 = 0$ case generates the least amount of lift, which is even less than that of the solid

airfoil. As β_1 increases, C_L continually increases, and it exceeds that of the solid airfoil. The maximum lift improvement over the solid case is around 3% for the case with $\beta_1 = 16$ deg. Also, all values of β_1 result in almost identical drag coefficients that are only slightly higher than that of the solid airfoil. Therefore, it is decided to use slots with small tilt angles in the remaining parts of the research.

Results and Discussion

In the Primary Results section, results of several simulations were presented. Even though the lift coefficient seemed to show some improvement as compared to the solid airfoil in the low AoAs, all of the slotted cases had an inferior performance at higher AoAs. Moreover, there seems to be an inevitable drag penalty observed for all of the cases even at low AoAs. After investigation of the velocity vectors near the slot inlet, it was decided to slightly lower the slot in order to allow it to capture more incoming air flow. The parameter h (see Fig. 3(*b*)) was therefore changed from 4 cm (0.04c) to 5.5 cm (0.055c). Also, based on the findings of the Primary Results section, a very mild inclination angle ($\beta_1 = 2$ deg) was applied to slot's first-leg, and it was maintained for all simulation cases, regardless of the value of other geometrical parameters and AoA. The intention was to help the slots with capturing more incoming air at higher AoAs. Similar to the Primary Results section, the influence of slot first-leg length, exit angle, and slot width was studied on lift and drag coefficients.

Effect of the First-Leg Length and Slot Width. Figure 9 shows how lift and drag coefficients change with AoA as the first-leg length varies between 10% and 80% of the chord length. For all three cases, the slot width and the exit angle of the second leg are maintained at $w/c = 0.01$ and $\beta_2 = 25$ deg, respectively. Note that all the cases show a superior performance as compared to the solid airfoil for AoAs as large as 10 deg. This performance is a testimony of definitely an improvement compared to the original slot design where the slot was drilled higher up (see Figs. 6 and 7,

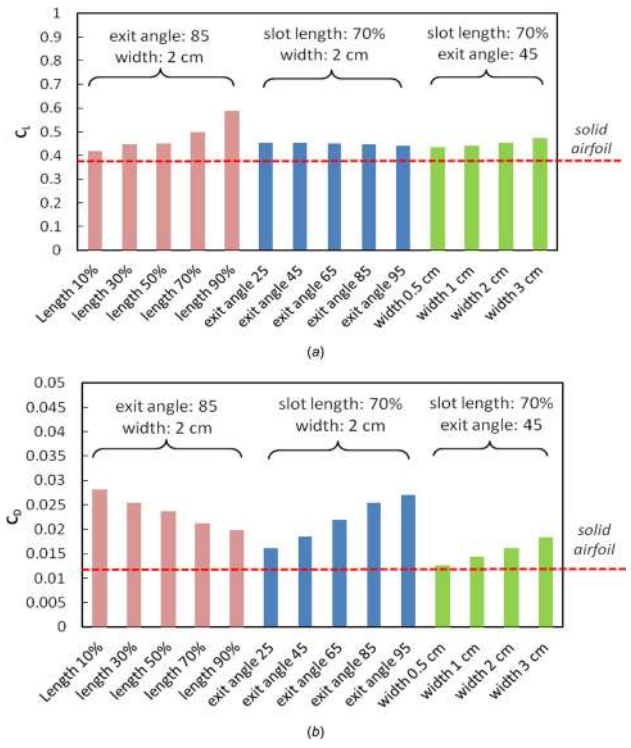

Fig. 5 Results of a parametric study on (*a*) lift and (*b*) drag coefficients, as a function of slot first-leg length, slot width, and the exit angle

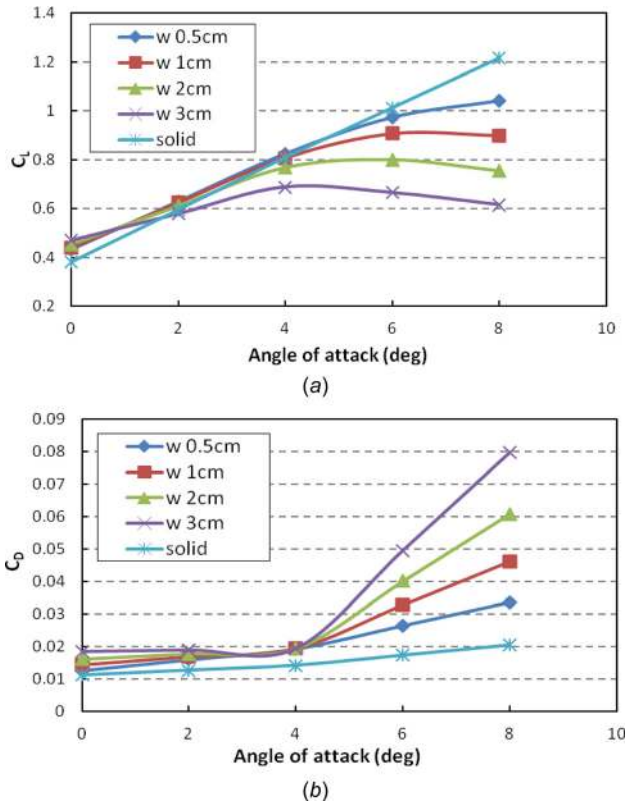

Fig. 6 Performance of slotted airfoils with different slot widths in terms of (*a*) lift coefficient and (*b*) drag coefficient

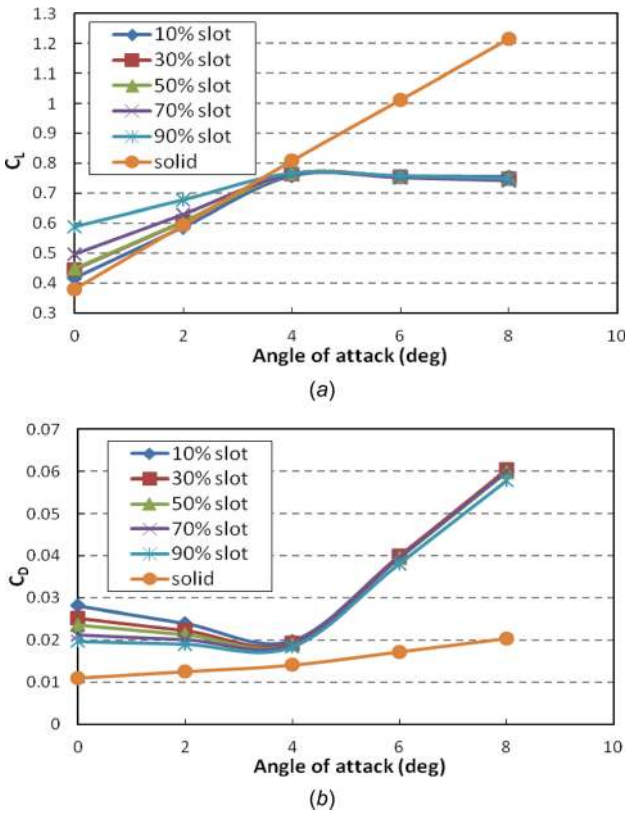

Fig. 7 Performance of slotted airfoils with different first-leg lengths in terms of lift and drag coefficients

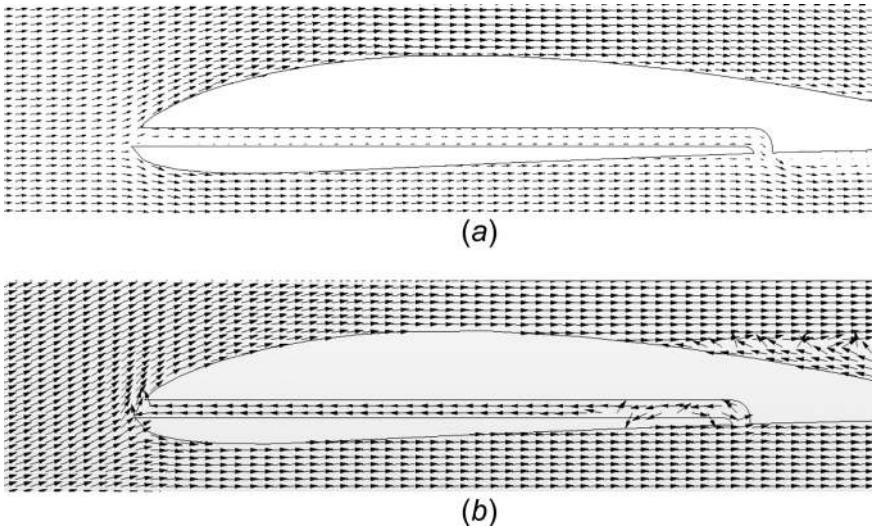

Fig. 8 Velocity vectors near a slotted airfoil with $L_1/c = 70\%$, $w/c = 2\%$, $\beta_1 = 0$ deg, $\beta_2 = 85$ deg, and $h/c = 4\%$ operating under (*a*) AoA = 0 deg and (*b*) AoA = 8 deg

where the performance of all the slotted airfoils started degrading at AoA = 4 deg and above). While the three slot lengths considered in Fig. 9 are showing similar behavior, it is decided to use the longest one ($L_1/c = 80\%$) due to its slightly higher lift and lower drag especially at higher AoAs. The only drawback of the long slot would be the need for more ductwork and plumbing in order to implement the slot inside the airfoil. However, the overall weight and the installation cost are not considered as objective functions in the present work and can be items of a future study. Despite the current findings, there is still room for improvements, so it is decided to explore the impact of slot width at different AoAs, while setting $L_1/c = 80\%$. Slot width is varied in a reasonable range: $w/c = 0.25\%$, 0.5%, 1%, and 2%. For practical reasons, widths beyond this range are not tested. For instance, for the slots narrower than 0.25% of the chord length in width, the air passage through the slot may become clogged up as a result of dust accumulation. Lift and drag coefficients at different AoAs for various slot widths are presented in Fig. 10.

As shown in Fig. 10, the choice of slot width does not play a crucial role in low AoAs as long as the length is selected correctly. For AoAs up to 8 deg, all the selected widths can result in lift coefficients that are anywhere between 5% and 30% higher than the solid counterpart. For higher AoAs, however, there seems to be some disagreement between the lift predictions of slotted airfoils with different widths. For AoAs between 10 deg and 14 deg, while the two narrowest slots still provide some advantage compared to the solid airfoil, the two widest ones start degrading in performance. For the highest AoA considered (16 deg, which is the near-stall condition), only the narrowest one seems to be better than the solid airfoil.

A similar behavior is observed for the drag coefficient. Airfoils with slot widths of $w/c = 1\%$ and 1.5% perform very poorly, while the other two maintain their acceptable performance even at the AoA = 16 deg. Neglecting the possible issue of slot clogging, the slotted airfoil with $w/c = 0.25\%$ seems to be the best option. This slot provides an average lift coefficient improvement of 7% (15% for AoA = 0 deg and 3.25% for AoA = 16 deg) with respect to the solid airfoil in the *entire range* of AoA examined, while it yields no drag penalty. Comparing the above results with those from Fig. 6 (similar study but with the slot drilled higher up inside the airfoil) reveals that the slot's vertical position can have a significant impact on the overall aerodynamic performance.

To provide more insights into the flow patterns around and through slotted airfoils, the contours of pressure and normalized velocity (U_i/U_∞) are presented in Fig. 11. One can note in Fig. 11(*a*) that the presence of the slot slightly below the stagnation point of the airfoil causes the high-pressure fluid particles (adjacent to the streamline hitting the airfoil nose) to find their way through the slot. The flow of the high-pressure air through the slot creates an upward force on the slot ceiling. Even though a similar force pushes down the bottom surface of the slot, due to the small difference between the areas of the two surfaces, the net force will remain upward. As a result, this contributes to few percent increase in lift. Another phenomenon contributing to the lift increase is the effect of the upward thrust force created on the airfoil because of the jet of air existing downward from the slot. Finally, this jet exiting the slot slows down the high-velocity streams of air flowing below the airfoil after mixing with it. The mixing effect causes a small local pressure rise, which in turn can contribute to few percent increase in the lift force.

Table 2 Lift and drag coefficients for slotted airfoils with different first-leg angles

Slot inlet angle β_1 (deg)	Lift coefficient	Drag coefficient
0	0.799	0.0143
4	0.825	0.0144
8	0.827	0.0147
16	0.832	0.0149
Solid airfoil	0.808	0.0141

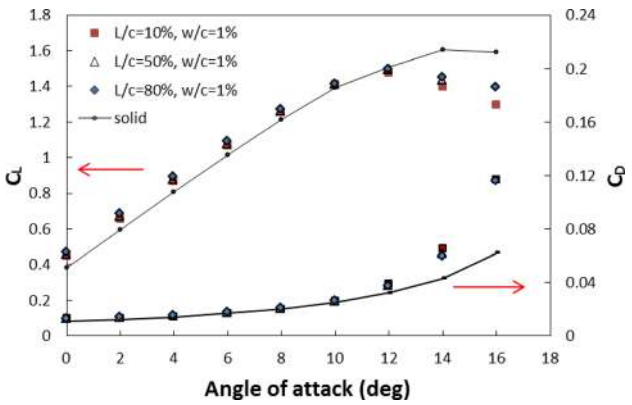

Fig. 9 Lift and drag coefficients of slotted airfoils with different first-leg lengths, $w/c = 1\%$, and $\beta_2 = 25$ deg at different AoAs

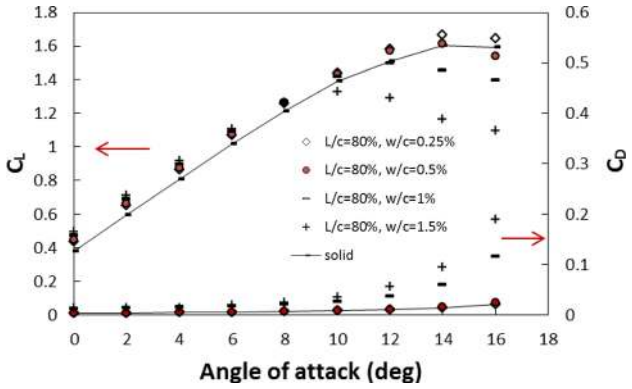

Fig. 10 Lift and drag coefficients of slotted airfoils with different slot widths, $L_1/c = 80\%$, and $\beta_2 = 25$ deg at different AoAs

Effect of the Slot Exit Angle. For a slotted airfoil with a near-optimal performance ($L_1/c = 80\%$ and $w/c = 0.5\%$), the influence of the *relative* exit angle of the second leg β_2 is studied. This angle can alter the pattern of mixing between the slot flow and the flow on the pressure-side near the trailing edge and, therefore, can contribute to the lift and drag coefficients. Three exit angles 10 deg, 25 deg, and 85 deg are considered, and the force coefficients are compared against the data from the solid airfoil in Fig. 12. For low to moderate AoAs, there is not a significant difference in the lift coefficients between the cases with different β_2 values. Only at near-stall AoAs (14 deg and 16 deg), the higher exit angle seems to result in a slightly higher lift. The same statement can be made regarding the drag coefficient. However, since the overall difference between the performance of slotted airfoils with $\beta_2 = 25$ deg and $\beta_2 = 85$ deg is not significant, it is decided not to change that angle for this research.

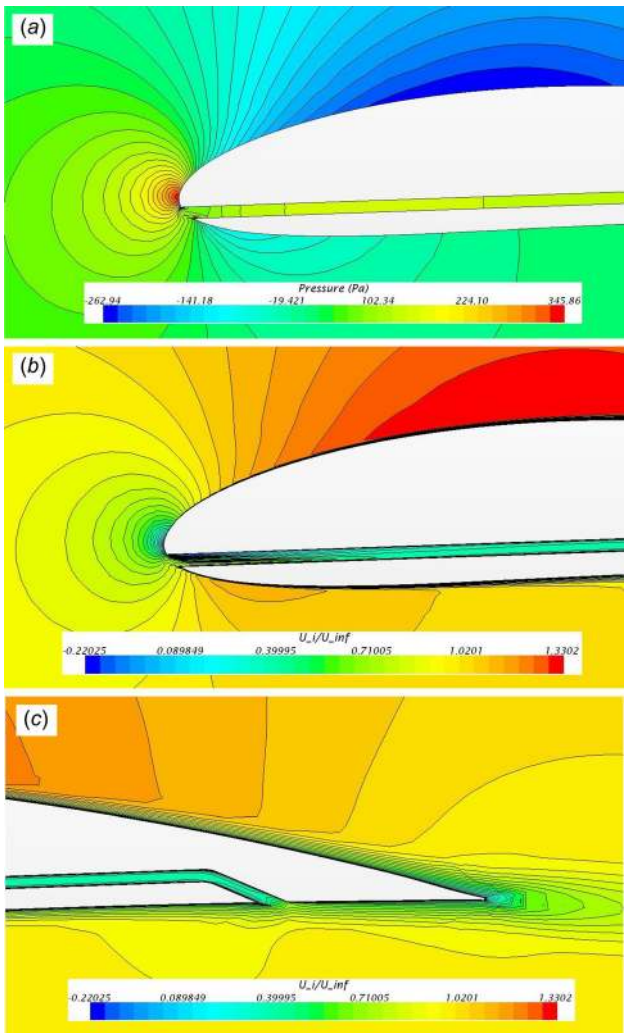

Fig. 11 Pressure contours (near leading edge) and normalized velocity contours (near both leading and trailing edges) for a slotted airfoil with $L_1/c = 80\%$, $w/c = 1\%$, $\beta_1 = 0$ deg, $\beta_2 = 80$ deg, and $h/c = 5.5\%$ at AoA = 0 deg

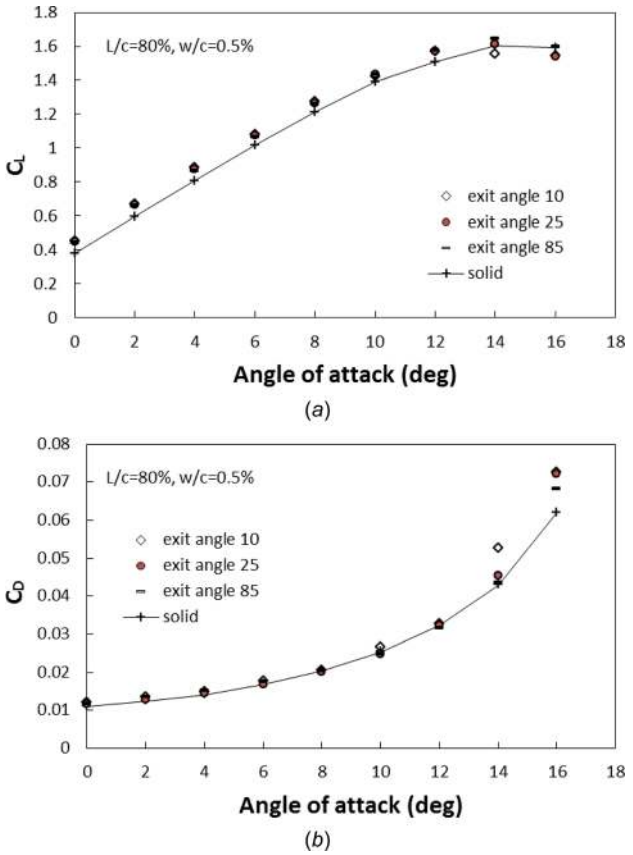

Fig. 12 Performance of slotted airfoils with different relative exit angles β_2, with $L_1/c = 80\%$, and $w/c = 0.5\%$: (*a*) lift coefficient and (*b*) drag coefficient

Conclusions

A novel passive flow control technique was introduced and investigated. A narrow span-wide slot was drilled near the leading edge of the airfoil, to draw some of the incoming air flows into the airfoil and eject it from the pressure-side. After an initial validation of CFD, a series of simulations were carried out for several combinations of slot geometrical parameters, such as slot first-leg length, slot width, and slot exit angle, and it was observed that lift could be improved under certain conditions.

For AoA = 0 deg, it was determined that all configurations could improve lift by 7–65%, while they all seem to come with a drag penalty. It was decided that the best performance is achieved when L_1 is kept as large as possible, and when slot width w_1 and β_2 are kept as small as practically possible. Despite the good performance at AoA = 0 deg, it was noticed that as the AoA increases, the proposed slotted airfoil could not show improvement compared to the solid airfoils. As a remedy for this problem, it was then decided to examine four different first-leg angles for operation under the AoA of 4 deg. Results indicated that even a small positive β_1 could help with the aerodynamic performance.

After following the streamlines near the airfoil leading edge, it was decided to lower the position of the slot so as to allow the slot

to capture more incoming air and at different AoAs. Therefore, in the next set of simulations, h/c was set to 0.055, and all cases were given a small inclination angle $\beta_1 = 2$ deg. Again, the impact of slot first-leg length, slot width, and slot exit angle was investigated. It was concluded that longer and narrower slots could provide the largest improvement with respect to the solid airfoil. For the most optimal configurations, an average lift coefficient increase by 7% was observed in the entire range of AoA, while there was no drag penalty.

Future Work

Several different research paths can be taken in future studies. First, the influence of other geometrical parameters of the slot can be assessed. To name a few, one can investigate the influence of slots with different vertical positions and different inlet angles, curved slots, and the impact of bell-mouth-shape slot inlet on the aerodynamic performance.

Based on a few important design parameters, it is possible to run an optimization routine to locate the optimum slot configuration for maximization of lift or lift-to-drag ratio. Optimization will be carried out for operation under a very small range of AoA, which is, in turn, determined based on the prevalent local air speed, the rotational velocity, and their corresponding uncertainties (for wind turbine applications).

Moreover, note that in the process of making a decision on the proper slot configuration, there may exist more objective functions involved in addition to the lift and drag coefficients. For instance, the extra weight due to the additional plumbing materials and the installation cost could be important factors. In the future studies, those factors can be taken into account.

Based on the findings of the optimization study, a new airfoil can be designed, fabricated, and tested inside a wind tunnel to verify the superiority of the optimal design as compared to other solid and slotted airfoils. Finally, once an optimal design is determined, one can simulate and analyze the flow over a rotating slotted wind turbine blade. Either reduced order models such as blade element momentum or a more sophisticated three-dimensional CFD simulation can be performed to examine the performance of slotted blades as compared to the conventional solid blades regarding torque and power generation.

Acknowledgment

The first author is very grateful for the financial support provided through the UWM Distinguished Dissertation Fellowship Award. Computational resources provided by the High-Performance Computing (HPC) center of UWM are also highly appreciated.

This research was currently funded by the U.S. Department of Energy (DOE) DE-EE0000545 and the National Science Foundation (NSF) CBET-1236312.

Nomenclature

A = planform area of the airfoil (m^2)
a_1 = constant used in Eq. (2) (default value: 0.31)
AoA = angle of attack (deg)
c = airfoil chord length (m)
C_D = drag coefficient
C_L = lift coefficient
C_p = pressure coefficient, defined as $2(P - P_\infty)/\rho U^2$
D = drag force (N)
F_1 = coefficient used in Eq. (4)
F_2 = coefficient used in Eq. (2)
h = vertical (normal to chord) distance between the bottom-edge of slot's inlet plane and a fixed point within the airfoil (m)
k = turbulent kinetic energy (m^2/s^2)
L = lift force (N)
L_1 = length of the first-leg of the slot (m)
P = pressure (Pa)
P_k = production of turbulent kinetic energy (m^2/s^3)
Re = Reynolds number, defined as $U_\infty c/\nu$
s = airfoil span length (m)
t = time (s)
T = temperature (K)
U = velocity vector (m/s)
$\langle u_i u_j \rangle$ = a Reynolds stress component (m^2/s^2)
w = slot width (m)
W = vorticity magnitude (1/s)
x = position vector (m)
y^+ = nondimensional wall distance for a wall bounded flow

Symbols

β = coefficient used in Eq. (4)
β_1 = angle between the slot first-leg and the horizontal line (deg)
β_2 = angle between the first and second legs of the slot (deg)
β^* = constant used in Eq. (3) (default value: 0.09)
γ = coefficient used in Eq. (4)
δ_{ij} = Kronecker delta
ε = turbulence dissipation rate (m^2/s^3)
μ_t = turbulent eddy viscosity (Pa·s)
ν = kinematic viscosity (m^2/s)
ν_t = turbulent kinematic eddy viscosity (m^2/s)
ρ = density (kg/m^3)
σ_k = coefficient used in Eq. (3)
σ_ω = coefficient used in Eq. (4)
$\sigma_{\omega 2}$ = constant used in Eq. (4) (default value: 0.856)
τ = shear stress (Pa)
ω = specific dissipation rate (1/s)

Subscripts

i, j, k = tensor index notations
t = turbulent quantities
∞ = free-stream

References

[1] Burton, T., Jenkins, N., Sharpe, D., and Bossanyi, E., 2011, *Wind Energy Handbook*, Wiley, Chichester, UK.
[2] Heathcote, D. J., Gursul, I., and Cleaver, D. J., 2016, "An Experimental Study of Mini-Tabs for Aerodynamic Load Control," AIAA Paper No. 2016-0325.
[3] Martin, S., and Bhushan, B., 2014, "Fluid Flow Analysis of a Shark-Inspired Microstructure," J. Fluid Mech., **756**, pp. 5–29.
[4] Bixler, G. D., and Bhushan, B., 2013, "Fluid Drag Reduction With Shark-Skin Riblet Inspired Microstructured Surfaces," Adv. Funct. Mater., **23**(36), pp. 4507–4528.
[5] Troldborg, N., Zahle, F., and Sørensen, N. N., 2015, "Simulation of a MW Rotor Equipped With Vortex Generators Using CFD and an Actuator Shape Model," AIAA Paper No. 2015-1035.
[6] Gao, L., Zhang, H., Liu, Y., and Han, S., 2015, "Effects of Vortex Generators on a Blunt Trailing-Edge Airfoil for Wind Turbines," Renewable Energy, **76**, pp. 303–311.
[7] Wang, C., and Sun, M., 2000, "Separation Control on a Thick Airfoil With Multiple Slots Blowing at Small Speeds," Acta Mech., **143**(3–4), pp. 215–227.
[8] Johnson, S. J., van Dam, C. P., and Berg, D. E., 2008, "Active Load Control Techniques for Wind Turbines," Sandia National Laboratories, Albuquerque, NM, Technical Report No. SAND2008-4809.
[9] Subash, B., Nithyapathi, C., Manikandan, D., and Murali, K. K., 2014, "Aerodynamic Optimization of Wind Turbine Blade by Employment of Slot to Counteract the Effect of Drag," Int. J. Emerging Technol. Adv. Eng., **4**(3), pp. 249–253.
[10] Ibrahim, M. S., Alsultan, A., Shen, S., and Amano, R. S., 2015, "Advances in Horizontal Axis Wind Turbine Blade Designs: Introduction of Slots and Tubercle," ASME J. Energy Resour. Technol., **137**(5), p. 051205.
[11] Alsultan, A., 2015, "Computational and Experimental Study on Innovative Horizontal-Axis Wind Turbine Blade Designs," M.Sc. thesis, University of Wisconsin-Milwaukee, Milwaukee, WI.
[12] Menter, F. R., 1994, "Two-Equation Eddy-Viscosity Turbulence Models for Engineering Applications," AIAA J., **32**(8), pp. 1598–1605.
[13] Wadcock, A. J., 1978, "Flying-Hot-Wire Study of Two-Dimensional Turbulent Separation on an NACA 4412 Airfoil at Maximum Lift," Ph.D. thesis, California Institute of Technology, Pasadena, CA.
[14] Rumsey, C., 2014, "2DN44: 2D NACA 4412 Airfoil Trailing Edge Separation," NASA Langley Research Center, Hampton, VA, accessed Aug. 27, 2016, http://turbmodels.larc.nasa.gov/naca4412sep_val.html